FABRICATION OF SEMICONDUCTOR NANOSTRUCTURED THIN FILM USING INKJET PRINTING

A Thesis

Presented to the Faculty of the Graduate School

of Cornell University

In Partial Fulfillment of the Requirements for the Degree of

Master of Science

by

Qiannan Wen

August 2017

ABSTRACT

Self-assembly of semiconductor nanocrystals into superlattice has opened up the materials library by design. Driven by the complex interplay between nanocrystal, ligand, solvent and substrate, integration of nanostructures into solid state devices needs to overcome difficulties in preserving surface stability of nanocrystals while maintaining the long range order of the superstructure. Here we demonstrate the fabrication of lead sulfide nanocrystals thin films using inkjet printing. Uniform thin films with monolayer to bilayer thicknesses with periodic arrangement of nanocrystals were obtained. Adding a liquid subphase to initiate the self-assembly at fluid interface increased the ordering range of the superlattice. Further improvements in the printing technique such as the compatibility with low viscosity ink and surface sensitive materials would advance the fabrication of single crystal nanostructured thin film.

BIOGRAPHICAL SKETCH

Qiannan Wen grew up in Ningbo, China. She graduated from City University of Hong Kong in 2015 with a Bachelor's degree in Materials Engineering. She finished her undergraduate dissertation in Prof. Andrey Rogach's group on optical properties of near-infrared quantum dots. In 2015, she came to Cornell University to pursue a Master's degree in Applied Physics. Prior to the study of nanocrystals assembly guided by Prof. Tobias Hanrath, she researched optical cavities in Prof. Jin Suntivich's group.

To my parents

ACKNOWLEDGMENTS

First, I would like to thank Prof. Tobias Hanrath for giving me the chance to work with him and his valuable guidance throughout the project. His encouragement meant a lot to me when the results were not that promising. I additionally thank other members in my committee, Prof. Jin Suntivich and Prof. Gregory Fuchs, for taking their time advising me in research and other aspects of my studies.

I am deeply grateful to Dr. Detlef Smilgies who provided critical help during the X-ray measurements. I was inspired by his enthusiasm looking at the fundamental science of how everything works. Thanks to his willingness to share his knowledge and experience, I learned a lot about the coating of nanostructured thin film.

I also appreciate the help from all my lab mates, without whom this project would have never proceeded on time. Jen-yu Huang and Eliad Peretz are experts on printing technologies. They shared their knowledge to me in this field and helped refine my experimental approaches. Doug Nevers and Jessica Akemi Cimada da Silva instructed me on the synthesis of nanocrystals and answered all my questions regarding the details of the chemistry. Kevin Kimura and Ben Richards always came at the right time troubleshooting the equipment when I had difficulties operating it. Also, I thank our group alumni, Dr. Kevin Whitham, Dr. Kaifu Bian and Dr. Ben Treml, who produced incredible work on quantum dots in the past years.

Finally, I would like to thank my family who have always supported me from a fifteen-hour-flight-away.

TABLE OF CONTENTS

LIST OF FIGURES

LIST OF ABBREVIATIONS

3d	three-dimensional
NC	nanocrystal
QD	quantum dot
QDS	quantum dots solids
TEM	transmission electron microscopy
SEM	scanning electron microscopy
GISAXS	grazing incidence small-angle X-ray scattering
HWHM	half width at half maximum
FWHM	full width at half maximum
EG	ethylene glycol
DCB	dichlorobenzene
EDA	ethylenediamine
BNSL	binary nanocrystal superlattice
C_8-BTBT	2,7-dioctyl[1]benzothieno[3,2-b][1]benzothiophene
TIPS-pentacene	6,13-bis(triisopro-pylsilylethynyl)pentacene
PDMS	poly(dimethysiloxane)
MPTMS	3-mercaptopropyltrimethoxysilane
PEG	2-[methoxy(polyethylenoxy)propyl]trichlorosilane
FFT	fast Fourier transform
FTIR	Fourier transform infrared
FCC	face centered cubic

1 Introduction

1.1 Semiconductor nanocrystals

Semiconductor nanocrystals (NCs), also called quantum dots (QDs), are the crystallites of size smaller than the Bohr radius of the exciton in bulk materials. The lowest excited state is dependent upon the size of NC approximated in Brus equation[1]

$$E = E_{Bulk\ BG} + \frac{\hbar^2\pi^2}{2R^2}\left[\frac{1}{m_e} + \frac{1}{m_h}\right] - \frac{1.8e^2}{\epsilon_2 R} + solvation\ energy\ loss$$

where $E_{Bulk\ BG}$ is the band gap of the bulk semiconductor, m_e and m_h are the effective mass of electron and hole, ϵ_2 and R are the dielectric coefficient and radius of the NC.

Quantum confinement leads to discrete energy states. Figure 1.1 (a) shows absorption spectra of lead sulfide (PbS) NCs. The redshift of the lowest absorption peak corresponds to the increasing size of NCs. PbS NCs can achieve strong quantum confinement in both electron and hole (exciton Bohr radius of 20 nm).[2] It has been applied to wide ranges of electronic devices including solar cells, photodetectors and light emitting diodes.[3–6]

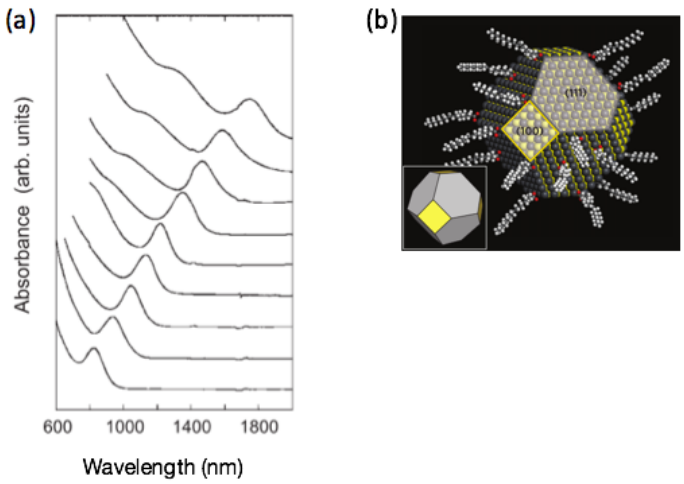

Figure 1.1 (a) Absorption spectra of PbS NCs with different sizes showing the quantum confinement effect on band gap. Spectra are offset vertically for clarity. (ref 2) (b) Illustration of truncated cube of PbS NC. Some ligands are removed for clarity. (ref 3)

The synthesis of NCs is performed in the general hot injection method that produces NCs with size distribution ~5-10%.[7–9] The nucleation and growth are mediated by the dynamic interactions between organic surfactants and the NC cores. Figure 1.1(b) shows a model of the PbS NC with its surface terminated by the (111) and (100) facets.[9] The surface is capped by oleic acid ligands for size stabilization.

1.2 Self-assembly of NCs

NCs with narrow size distribution may form periodic arrangement during solvent evaporation. The self-assembly of NCs is driven by the complex interplay among NC core, ligand, solvent and the environment. Usually the assembled structures have weak interaction between NCs

building blocks. Partial removal of the ligands induces epitaxial bonding between facets and forms quantum dots solids (QDS). The collective properties of the QDS can be tuned flexibly by the building blocks and the assembly symmetries.

Figure 1.2(a) is a TEM image of PbSe QDS with epitaxial connection between (100) facets of the individual QD and figure 1.2(b) shows the transport measurements on a field-effect transistor by Whitham et al.[10] They observed that the electron and hole mobility was significantly limited by the variations in the epitaxial connections between neighboring facets, and claimed that a complete electron delocalization can be realized in the superlattice with uniform bonding between individual particles based on their theoretical calculations.[10]

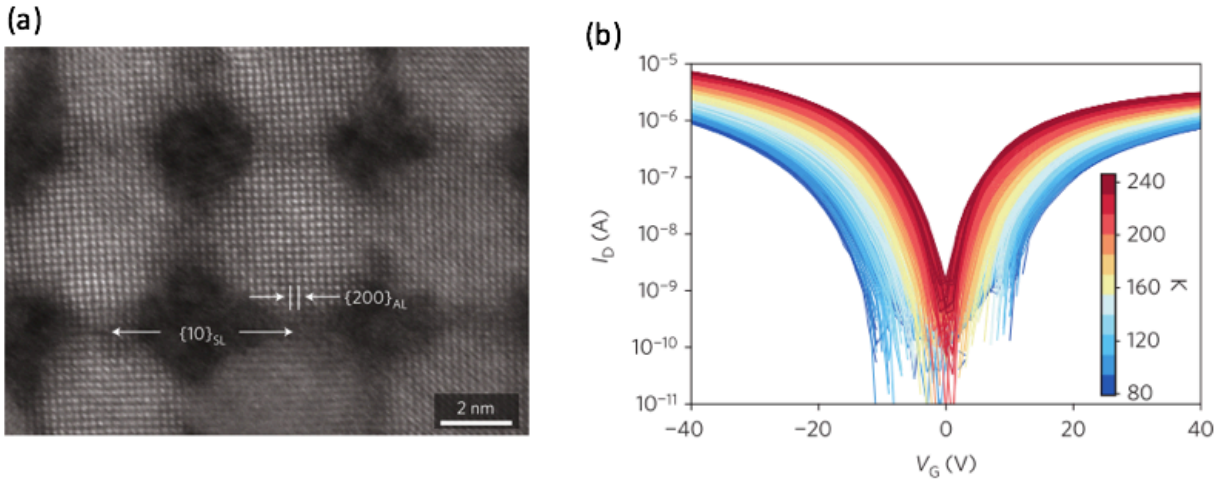

Figure 1.2 (a) High resolution TEM image of PbSe QDS showing bonding connections between NCs. The average size of individual NC is 6.5 nm. (b) Transport measurements on a field-effect transistor made from PbSe QDS. (ref 10)

There have been rigorous theoretical investigations in the electronic properties of QDS.[10–13] Kalesaki et al.[12] reported the existence of Dirac bands and topological states in the graphene type lattice of CdSe QD, and that the electronic structure of the individual QD contributes to the distinct QDS band structures that are not found in a normal solid. Different symmetries of PbSe NCs superlattices have been synthesized by Evers et al.[14] by changing the reaction temperatures and ligand densities. However, the fundamental mechanism of oriented attachment is unresolved. The fabrication of long range ordered QDS with uniform bonding between neighboring particles is still an experimental challenge.

1.3 Single crystal thin film deposition

Nanostructured thin films with large domain sizes are critical to electronics applications. While there has been enormous studies on the coating of organic materials[15–18], the processing-structure relationship is less understood in the NCs based thin films.

Dong et al.[19] proposed the method of liquid interfacial NCs assembly where the NCs solution was added onto a chemically inert subphase (for example, diethylene glycol). The assembled layer of binary nanocrystal superlattice (BNSL) at liquid-air interface can either be transferred directly to a solid substrate as shown in figure 1.3(a), or via a poly(dimethysiloxane) (PDMS) mold in the Langmuir-Schaefer method shown in figure 1.3(b) as reported by Paik et al.[20] They showed that by structuring the PDMS mode into meso- and microscale patterns, the assembled

superlattice could be patterned in the same way and the ordering range of the superlatttice was preserved (domain size ~900 nm).

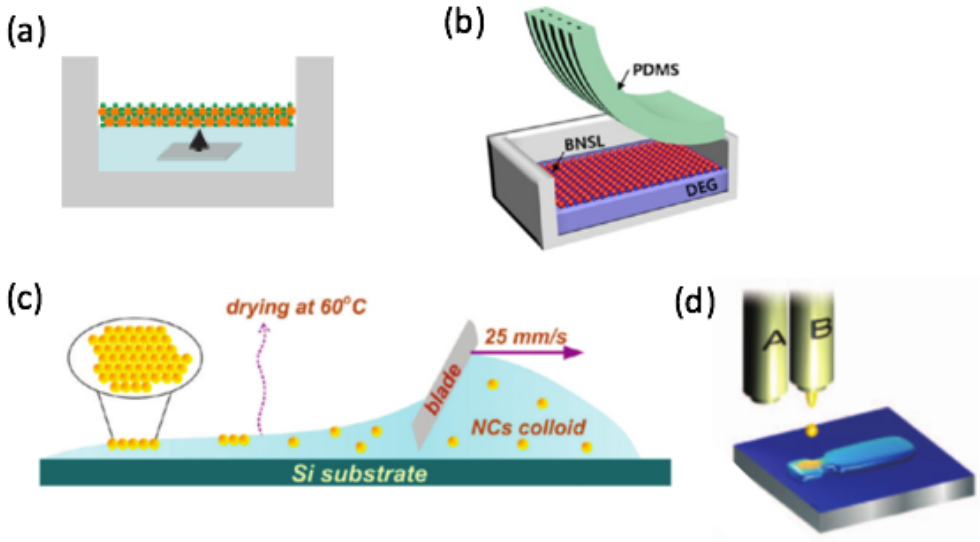

Figure 1.3 Illustration of NCs thin film deposition methods. (a-b) Liquid-air interface assembly of BNSL followed by (a) film transfer from the bottom; (ref 19) (b) Langmuir-Schaefer transfer to a PDMS mode. (ref 20) (c) Doctor Blading of NCs thin film coating on a large area. (ref 21) (d) Double-head inkjet printing of organic molecules onto a patterned silicon substrate. (ref 15)

Doctor Blading is a large-area coating technique. As shown in figure 1.3(c), the blade moves at a constant speed over the NCs solution at a certain gap from the substrate. Wu et al.[21] reported the fabrication of magnetic NCs thin film with grain size ~1 μm. A similar solution shearing method was applied to deposit thin films of aligned crystals of 6,13-bis(triisopro-pylsilylethynyl)pentacene (TIPS-pentacene) in the channel region of a transistor by Park et al.[17]

Inkjet printing has received attention for years. Minemawari et al.[15] reported the formation of single crystal of 2,7-dioctyl[1]benzothieno[3,2-b][1]benzothiophene (C_8-BTBT) thin film using a double-head inkjet printer presented in figure 1.3(d). The shape of the pattern was shown to be effective in guiding the crystal nucleation and growth.

1.4 Thin film characterization techniques

Nanostructured thin films are characterized by optical microscopy, transmission and scanning electron microscopy (TEM and SEM), atomic force microscopy (AFM), or the diffraction based characterization, X-ray scattering. Grazing incidence small-angle X-ray scattering (GISAXS) is a powerful technique probing thin film in an extensive view of about ~mm^2 and gives quantitative analysis on the structure.[22] Figure 1.4 illustrates the setup in a GISAXS measurement. The incident X-ray beam at an angle of α_i to the substrate, labelled with its wave vector k_i, is scattered off the monolayer thin film with periodically arranged NCs. The scattering beam k_f reaches the detector at an angle α_f and $2\theta_f$ in the vertical and horizontal directions, and creates a peak, in this case the Bragg rod in the q-plane. The peak position is determined by the periodic ordering in each direction. The scattering intensity is influenced by the substrate roughness, NCs size, shape distributions and the assembly ordering.

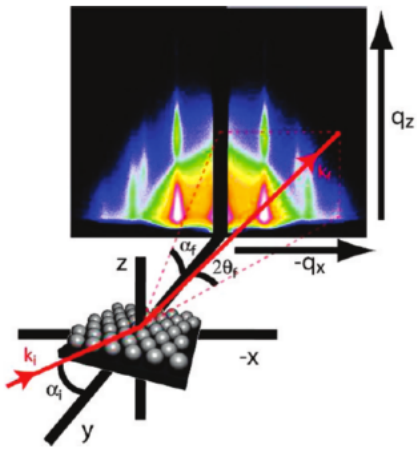

Figure 1.4 Illustration of GISAXS measurement of a NCs monolayer film. The scattering pattern is shown in the q-plane. (ref 22)

2 Self-assembly of NCs on a solid substrate

2.1 Introduction

Printed electronics is of interest due to its features including low cost, drop-on-demand, compatibility with flexible substrates and large scale fabrication.[15] The Dimatix Materials Printer used in this study is a piezo driven inkjet printer with droplet size 20-50 μm and displacement accuracy ~20 μm. The jetting profile depends on viscosity and surface tension of the liquid.

Inkjet printing has been demonstrated in organic thin film fabrication with great achievements.[15,23,24] Minemawari et al.[15] demonstrated the printing of single crystal C_8-BTBT thin film using an anti-solvent to control the rate of nucleation and solvent evaporation, and showed that the directed liquid flow from a protuberant area to wider regions facilitated the singly crystal growth. Li et al.[24] reported that the single crystal growth of C_{60} could be aligned with solvent receding using an extra pinner structure on the substrate. The inkjet printing with ink resolution of picoliter allows control of liquid diffusion and precise registry of the materials on a defined area.

The printing of inorganic NCs has been less addressed due to the limited materials compatibility and the difficulties in forming ordered structures. Common methods of NCs thin film fabrication such as drop casting, spin coating, Langmuir-Schafer, and Doctor Blading have been shown to obtain long range ordered NC assembly structures.[9,19–21,25]

Choi et al.[26] demonstrated the fabrication of an all-NCs field-effect transistor with a combination of metal, semiconductor and oxide NCs through multiple steps of photolithographic patterning, spin coating and ligand exchange. The development of printing technique is an essential step towards the integration of colloidal materials into electronic circuits.

Here we demonstrate the formation of ordered arrangements of PbS NCs at liquid-substrate interface using inkjet printing. NCs thin films with monolayer to bilayer coverages were obtained by optimizing the droplet placement. We compared the NCs assembly ordering on substrates functionalized with a short thiol group and hydrophilic group. SEM and GISAXS characterizations were used to probe superlattice structures.

2.2 Results and Discussion

2.2.1 Self-assembly of PbS NCs

One of the simple methods preparing NC superlattice is to drop cast diluted NCs solution on a solid substrate and let it dry with slow solvent evaporation. The deposit is usually non-uniform with ring stains, cracks and significant variations in thickness. These problems might be overcome by inkjet printing which enables controlled droplet placement and metering.

We printed PbS NCs solution on an un-patterned silicon substrate deposited with a layer of mercaptopropyltrimethoxysilane (MPTMS). The PbS NCs capped by oleic acid were suspended in dichlorobenzene (DCB) at 5 mg/ml, sonicated for 1 min and loaded into the Dimatix cartridge.

The standard deviation of NCs size was about 6%. The temperatures of the ink and platform were both set at 28 °C. The waveform was adjusted to dispense each droplet ~5 pL at 2 m/s from the height of 250 μm onto the substrate. The droplet spacing was 10 μm. We printed NCs solution of 10 nL, and then over-deposited with a second layer after it had dried. The sample was dry within 1 min. Figure 2.1(a) shows the GISAXS pattern of the deposit indexed to a face centered cubic (fcc) superlattice using the software from Smilgies.[27] The superlattice had a lattice constant of 14.3 nm, with the (111) plane parallel to the substrate and a 4% shrinkage in the vertical direction. Un-indexed scattering peaks might be related to another crystal orientation. The distance between neighboring NCs was about 3.5 nm, the separation by two ligand shells.

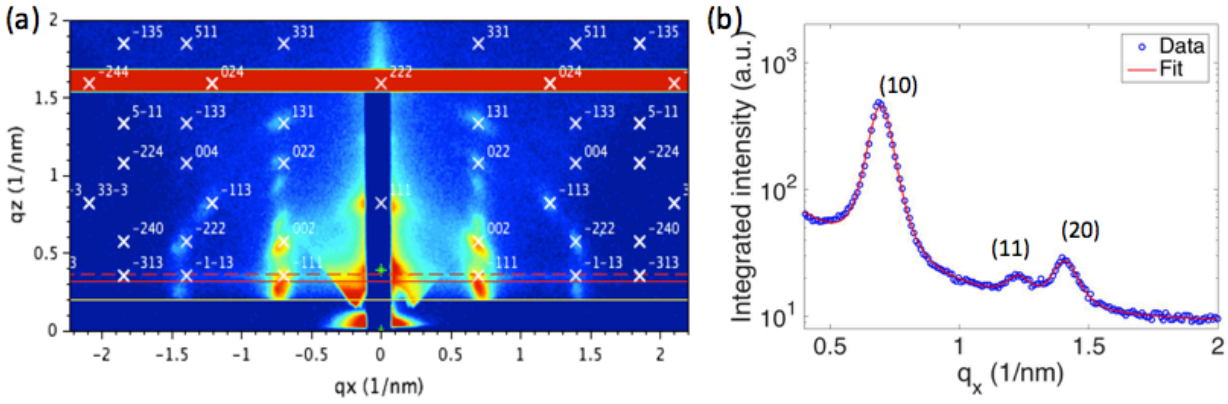

Figure 2.1(a) GISAXS pattern of a superlattice formed with PbS NCs suspension printed on Si/MPTMS without patterning. The white crosses are indices of fcc lattice. The red solid line is the film critical angle and red dashed line is the substrate critical angle. The yellow line is the horizon. (b) Vertically integrated intensities from the raw data (blue circle) and Lorentzian fit (red solid line) after exponential background subtraction.

The integrated scattering intensities along the in-plane (q_x) direction are shown in figure 2.1(b). The curve was fitted to three Lorentzian peaks. The (10) peak had half width at half maximum(hwhm), γ, of 0.044 nm^{-1}, and the grain size was estimated to be ~64 nm using the Scherrer equation $L = \pi K/\gamma$ (L is the grain size, K is the Scherrer constant taken to be 0.9).[28] This is close to the maximum resolvable grain size of the somewhat divergent microbeam.[29]

The crystallization of the NCs into 3d superlattice indicated the narrow size distribution of particles and preserved ligands. In other experiments we found that the deposition of multi-layered films ended up with smaller grain size and that different layers were uncorrelated. Thus we suspected that the well-ordered 3d lattice might be at the ring stains. The strategy of using coffee ring effect[30] to induce nucleation has been shown to deposit crystalline structures on a defined area.[16]

2.2.2 Inkjet printing of PbS NCs thin film

While it is straightforward to form NCs superlattice by a simple drop casting given the narrow size distribution of NCs, thin film coating on a confined micrometer-sized pattern with small structural variations is challenging.

We used the inkjet printing to deposit NCs on a patterned substrate. A silicon substrate with a layer of oxide was patterned into various shapes with dimension of 100-1000 μm. The exposed areas were coated with a layer of MPTMS or PEG. (Details of substrate preparations are included in 2.2.4.) The PbS NCs in DCB (5 mg/ml) were printed on the patterned region and

dried in the printer chamber (temperature of 28 °C). The photoresist was removed with acetone in an ultrasonic bath for 10 s, rinsed with ethanol and dried with nitrogen. Figure 2.2 (a,c) show the optical images of the thin films printed with 100×20 droplets separated at 10 μm on a rectangular pattern deposited with MPTMS and PEG respectively. Figure 2.2 (b,d) are the thickness line scans performed on a P10 profilometer. The stylus force was 6 mg and the scan speed was 5 μm/s over the length of 250 μm (~half width of the pattern). Most regions in the pattern had uniform coverage of approximately monolayer to bilayer.

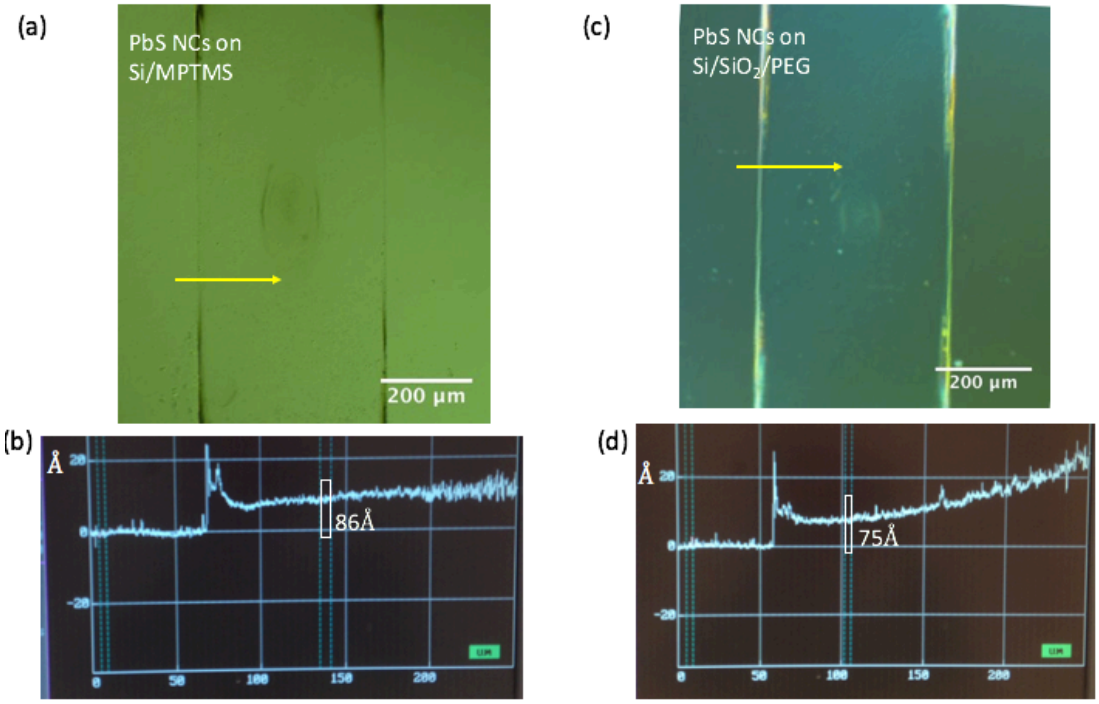

Figure 2.2 Optical image of a thin film printed on (a) Si/MPTMS and (c) Si/SiO_2/PEG. (b,d) Thickness line scan performed at the location marked by the yellow arrow in (a,c).

Figure 2.3(a) shows a SEM image of the thin film printed on Si/MPTMS. The grey regions and white regions are monolayer and bilayer structures, and the darkest regions are the voids. The

GISAXS data in figure 2.3(b) was obtained from a sample prepared in the same way. (There was oxidation and contamination that affected the SEM imaging, so the sample was prepared again.)

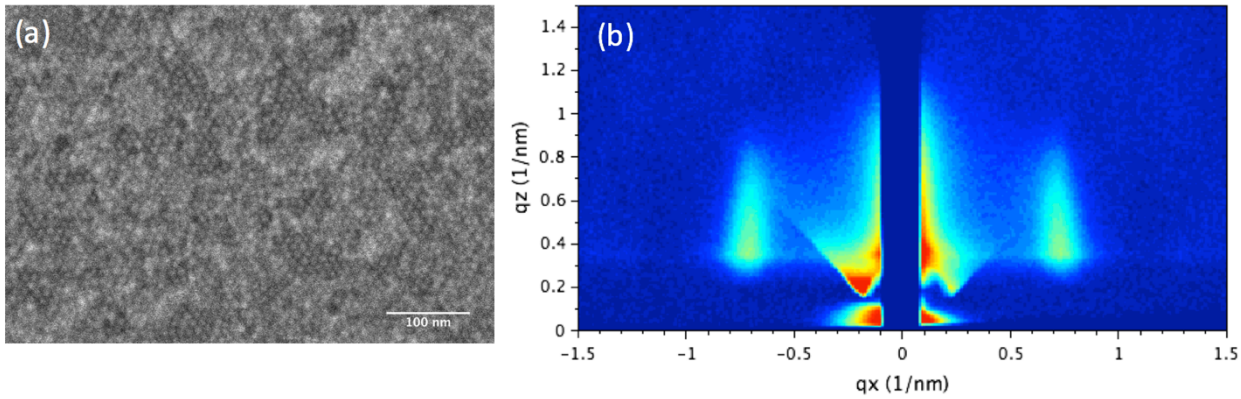

Figure 2.3 Characterization of PbS NCs thin film. (a) SEM image and (b) GISAXS pattern.

The GISAXS was measured at D1 station of Cornell High Energy Synchrotron Source (CHESS). The printed PbS NCs film was dried before placed on an open stage. The X-ray beam was of wavelength of 0.117 nm and incident at 0.25° on the thin film. The scattered beam was detected by a Pilatus 200K detector at a distance of 1013 mm. The exposure time of all samples in this chapter was 1 s.

The Bragg rod in the scattering pattern indicates ordered NCs arrangement in monolayer. The peak position along the q_x is related to the average particle spacing though the equation $d_{NC} = 2\pi/q_{max}$, where d_{NC} is the d-spacing and q_{max} is the peak position. From this pattern we calculate the d_{NC} to be 8.7 nm and the distance between nearest NC surface, δ, to be 3.4 nm (core size of NCs, d_{core}, ~ 6.6 nm) through the equation $\delta = \sqrt{\frac{4}{3}} d_{NC} - d_{core}$. This is slightly smaller than twice the length of oleic acid ligands (~1.8 nm).

We performed X-ray microbeam scan across the pattern. The integrated intensities along q_x are shown in figure 2.4(a), and inset is a schematic of X-ray measurement setup. The length of the sample illuminated by X-ray was 1 mm. Different positions on the pattern are plotted with variant colors. The d-spacing plotted in figure 2.4(b) is the averaged particle spacing obtained from the fitting of peak positions, with errors including only the uncertainties in Lorentzian fitting. A more complete structural factor needs to be considered to decouple the variations in lattice disorder relative to a perfect hexagonal lattice.[22] The particle spacing was slightly smaller near the edge, but overall the film was quite uniform. The average grain size was estimated from the peak width to be 40-50 nm.

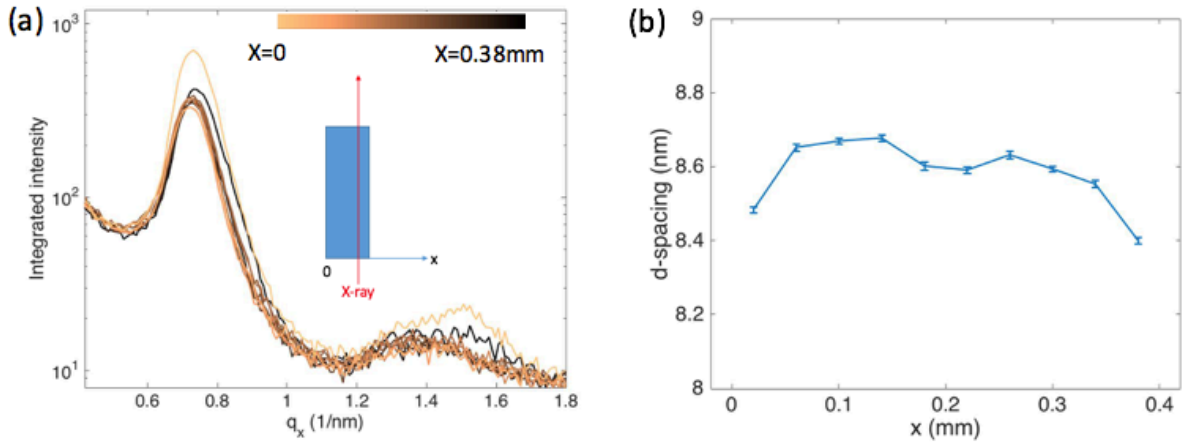

Figure 2.4 GISAXS microbeam scan of the PbS NCs thin film deposited on Si/MPTMS. (a) Vertically integrated intensities at different locations. Inset is the experimental setup showing X-ray direction and sample translation along x axis. (b) d-spacing calculated from peak positions in (a). The errors bars are the uncertainties in Lorentzian fitting.

On a substrate functionalized by the hydrophilic group of PEG, the thin film was printed under the same conditions. Figure 2.5(a) is an optical image of the sample. We performed X-ray scan at a step of 50 μm. Among them three locations are marked and the corresponding scattering patterns are presented in figure 2.5(b-d). The main feature of the scattering rods indicates the monolayer of NCs assembly.

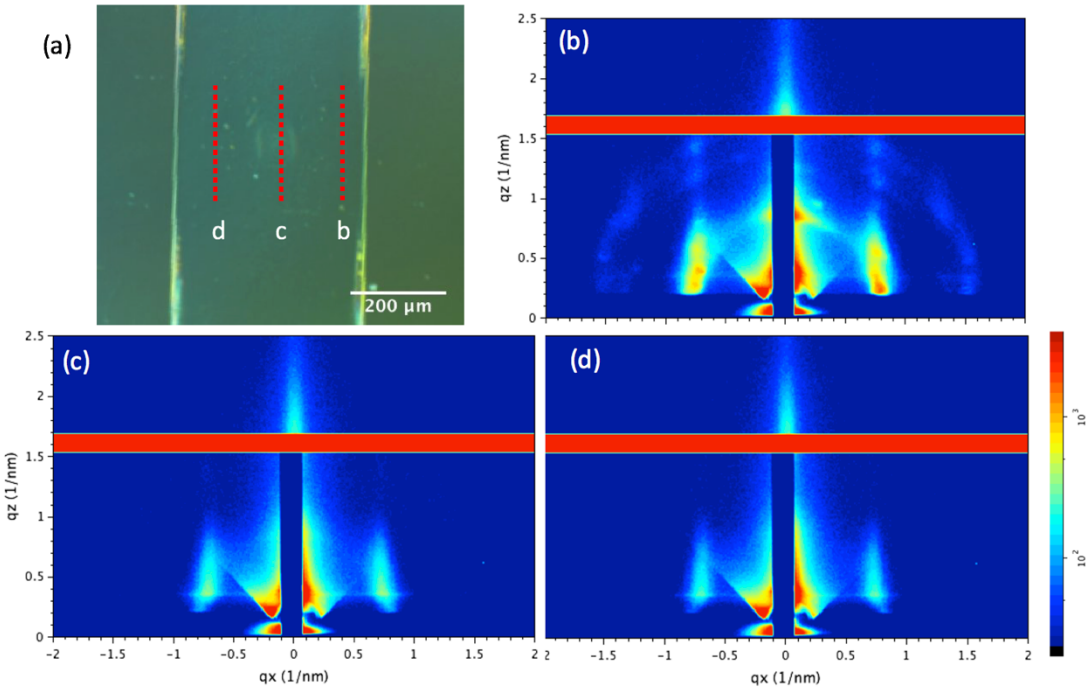

Figure 2.5 GISAXS microbeam scan on a PbS NCs thin film deposited on Si/SiO_2/PEG. (a) Optical image showing the positions where the GISAXS data in (b-d) were collected.

We calculated the d-spacing variations on this pattern, and compared it with two other samples prepared in the same way in figure 2.6. The particle spacing was consistently smaller towards the edge. As PEG is a hydrophilic group, the NCs had weaker interactions with the substrate, than to

the thiol group on Si/MPTMS. However, the average grain sizes were all in the range of 40-50nm.

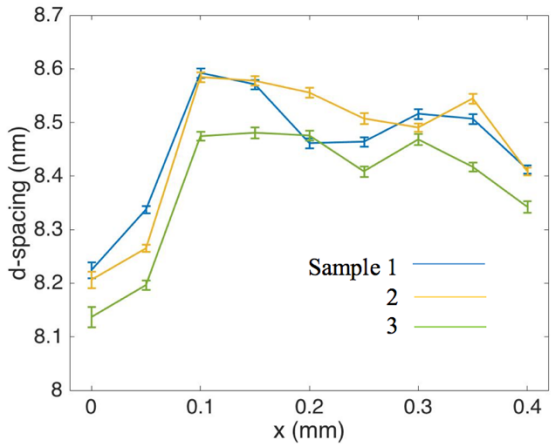

Figure 2.6 d-spacing calculated from GISAXS data of three samples prepared in the same way showing the consistent trend of particle distance. The errors bars are the uncertainties in Lorentzian fitting.

Figure 2.7(a-b) show the SEM image of the deposit on PEG treated substrate at different locations on the pattern. The film was about monolayer to bilayer as shown in figure 2.7(a) in most regions, and near the center it was thicker but with large voids in figure 2.7(b). As the thin layer near the edge was attached directly to the substrate, the reduced particle distance might be due to slight ligand perturbation by the -OH group in PEG on the substrate. The multi-layer structures near the center had more fraction of the NC-NC attachment and the nearest particles are separated by the ligand shell.

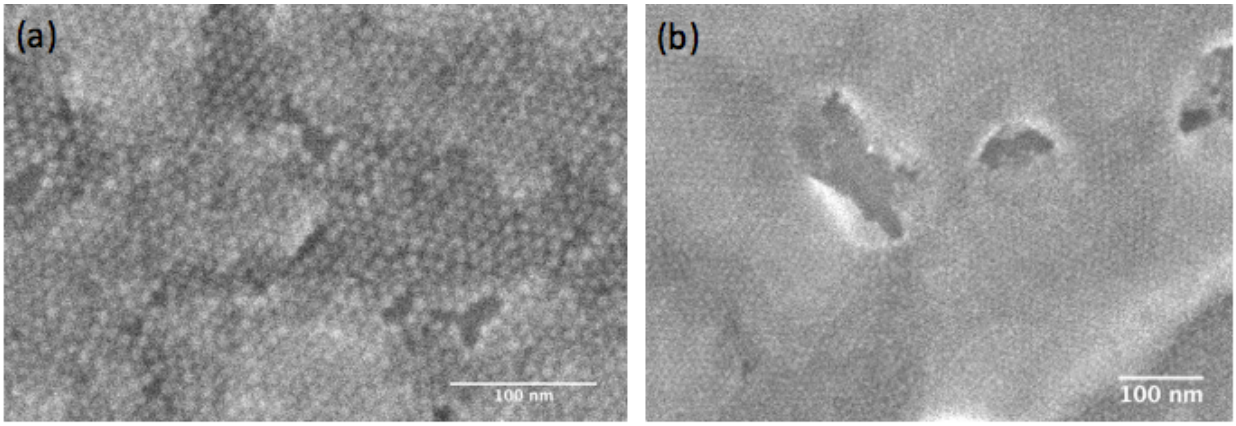

Figure 2.7 SEM images of a thin film on PEG deposited substrate (a) in an averaged region and (b) near the center of the pattern.

In NC based electronic devices, the long chain ligands need to be replaced with shorter chains to improve dot coupling and carrier transport. Choi et al.[30] reported the solution phase ligand exchange of CdSe QDs to thiocyanate before assembly, but formed glassy structures. The removal of ligands from a solid NCs thin film, usually introduces voids and cracks due to the reduction in ligand volumes. The in-situ ligand stripping during assembly may reduce particle distance while preserve the NCs ordering.[31] Extending this idea to NCs assembly on a solid substrate with self-assembled monolayer that specifically targets the ligands might have a better control on NCs surfaces by tuning the thickness and components of the functional group.

2.2.3 Thin film morphologies and defects

One of the problems in thin film deposition is the void formation. It may not be overcome simply by increasing the concentration of the solute. Figure 2.8 (a-d) show SEM images of the PbS NCs

film on Si/MPTMS. The void size was about 10-20 nm in a thin layer as shown in figure 2.8(a). As NCs were carried in the solvent during its receding, a thicker deposit was formed as shown in figure 2.8(b). There was an array of pores in this region with dimension of 50-200 nm in figure 2.8(c). Figure 2.8(d) is a magnified image of the multi-layer stack and the inset is the fast Fourier transform (FFT) showing hexagonal arrangement of NCs.

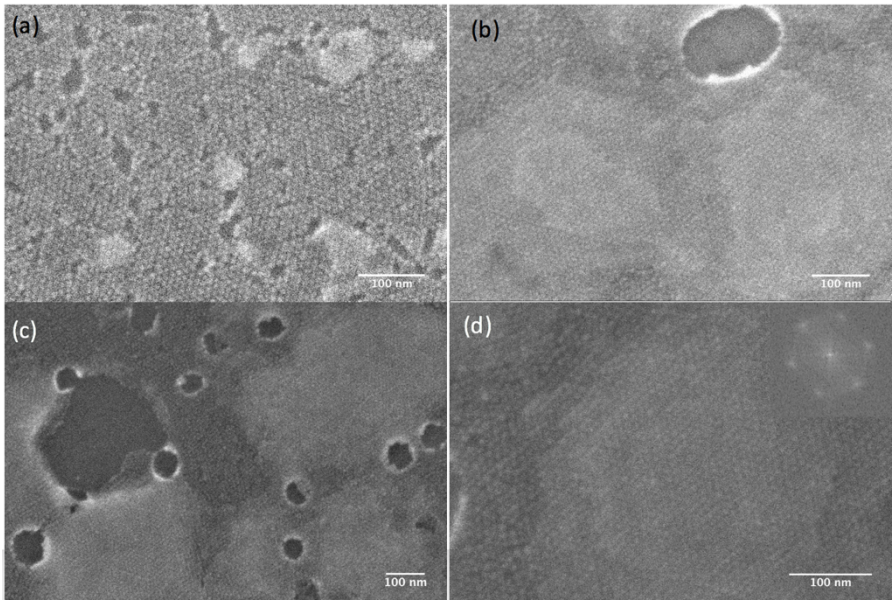

Figure 2.8 SEM images showing structural variations from (a) sub-monolayer to (b) multi-layer stacks. (c) Formation of an array of pores in the multi-layer deposit. (d) A magnified stack showing spatial variations between layers. Inset is the FFT showing hexagonal geometry.

A zoomed-in picture in figure 2.8(d) shows that the width of each layer decreased from bottom to the top, and that the growth of each layer was isotropic. Sigman et al.[32] reported the formation isotropic mound structures during assembly of gold nanoparticles dried from hexane. The nucleation cluster was captured on top of the mound and each layer had a smaller width than the

underlying layer, which is similar to the structure shown here. As the NCs superlattice nucleation was initiated at the liquid-solid interface, formation of scattered islands was due to the heterogeneous nucleation during fast supersaturation.

Interestingly, other than the large pore arrays formed among multi-layered film, we observed the inverse structures where the ordered multi-layer stacks formed in a thin film with their surroundings depleted of NCs.

The film was prepared by drop casting of 10 μl PbS NCs in DCB at 3mg/ml dried in a few hours. Figure 2.9(a-d) show SEM images of the deposit. Most areas were covered by multiple layers of NCs as shown in figure 2.9(a). In a small region on the substrate in figure 2.9(b), ordered multi-layer stacks formed. Figure 2.9(c) is a magnified image of the mound with small spatial variations between layers of NCs. Near the edge of the mound, we see from figure 2.9(d) that NCs were almost depleted, and further from it the coverage increased from sub-monolayer to multiple layers.

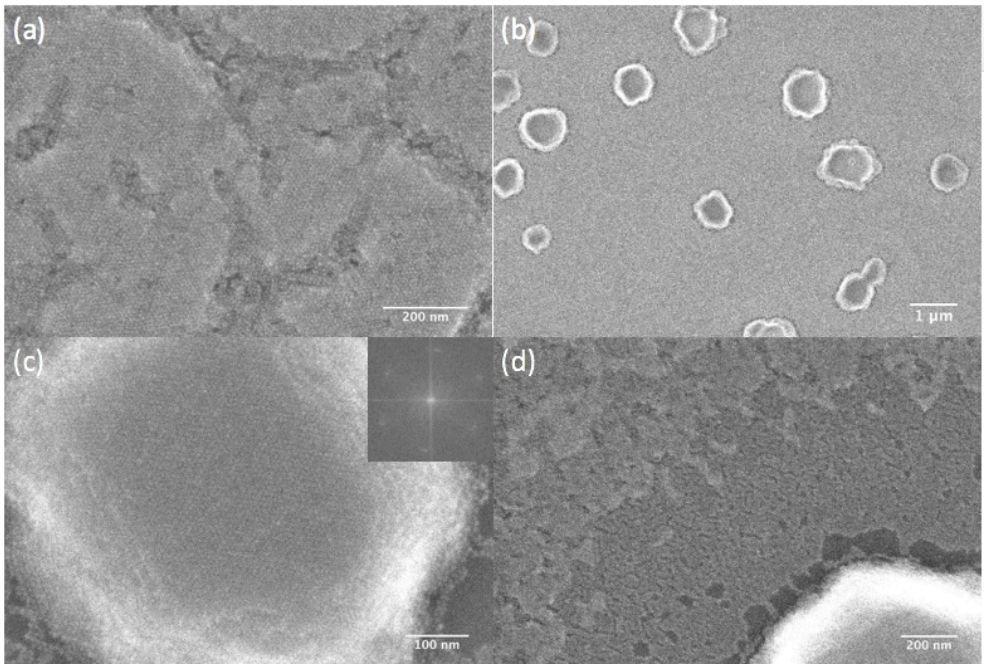

Figure 2.9 SEM images of the drop casted thin film. (a) Multiple layers formed in most regions; (b)Mound structures formed in a small region where the substrate was slightly contaminated. (c) A magnified image of the mound and its FFT in the inset. (d) Film morphologies near the mound.

Hanrath et al.[33] reported the formation of ravioli-shaped supracrystals during spin coating of PbSe NCs but only for high concentration NCs dispersion (50 mg/ml) and those structures showed square symmetry. Sigman et al.[32] also showed that in the assembly of gold NCs dried from toluene, mound structures formed at room temperature, while at elevated temperature the film became flatter. While such structures might be triggered by multiple parameters such as solvent, drying rate and substrate treatment, we found that the substrate had slight contaminations in the area these mound structures were formed. The multi-layer ordered stacks might be triggered by specific molecules. Applying slight perturbations to the substrate on which NCs assemble would give further insights into their formation mechanisms.

2.3 Conclusions

We used inkjet printing to deposit nanostructured thin film directly on patterned substrates. PbS NCs capped by oleic acid were assembled into hexagonal geometry after printed onto solid substrates. GISAXS microbeam scan of the thin film showed uniform assembly ordering across the pattern. The grain size of the assembly was limited to ~50 nm due to the fast evaporation and strong NC-substrate interactions.

The formation of NC thin film with approximately monolayer thickness is strongly affected by the substrate. Depositing a layer of functional group on the solid surface perturbs the NCs assembly environment. Further studies on the interaction between micrometer-sized droplet and the functional groups that specifically targets the surface chemistry of NCs, would unravel substrate effects in the coating of NCs film, and give insights into guiding superlattice growth on a soft substrate.

2.4 Experimental methods

2.4.1 PbS NCs synthesis

PbS NCs were synthesized using the method reported by Hines et al.[7] In a typical synthesis, 20 ml of oleic acid was degassed and heated with 450 mg of lead oxide powder in a 50 ml 3-neck flask. The temperature was increased to 150 °C and kept for an hour. 10 ml of 1-octadecene was degassed, transferred to nitrogen glovebox (oxygen level under 1 ppm) and mixed with 210 μl of hexamethyldisilathiane to form sulfide precursor. The temperature of the Pb-oleate was lowered to 130 °C before rapid injection of the sulfide precursor under rigorous stirring. The solution turned dark within 5 s. The reaction lasted for 65 s and was quenched to room temperature using a water bath. The products were washed with ethanol and re-dispersed in hexane three times. After the last washing, the products were dried under nitrogen flow and transferred to nitrogen glovebox for storage.

The absorption spectrum of PbS NCs was measured by dissolving dried NCs in tetrachloroethylene (TCE). Figure 2.10 shows the absorption spectrum obtained on a Cary-5000 UV-Vis-NIR spectrometer. The first exciton peak was fitted into a Gaussian curve with the peak position at 1708 nm and full width at half maximum, fwhm, of 138 nm. The average NCs size was calculated using the sizing curve $E_0 = 0.41 + \frac{1}{0.0252d^2+0.283d}$ from Moreels et al.[34] to be 6.9$\pm$0.4 nm, where E_0 is the energy of first absorption peak in eV, d is the particle diameter.

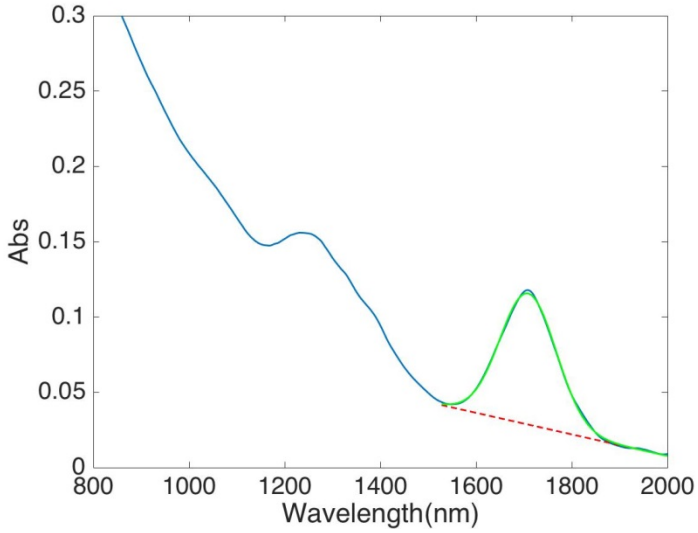

Figure 2.10 Absorption spectrum of PbS NCs suspended in TCE as measured (blue line), and the Gaussian fitting (green line) after linear background subtraction (red dashed line).

TEM characterization was performed using a FEI T12 Spirit TEM. Figure 2.11(a) shows a TEM image of the PbS NCs, and the diameter was estimated to be 6.6±0.4 nm from the statistics of 220 particles in figure 2.11(b). This presents a 0.3 nm offset from the absorption peak fitting.

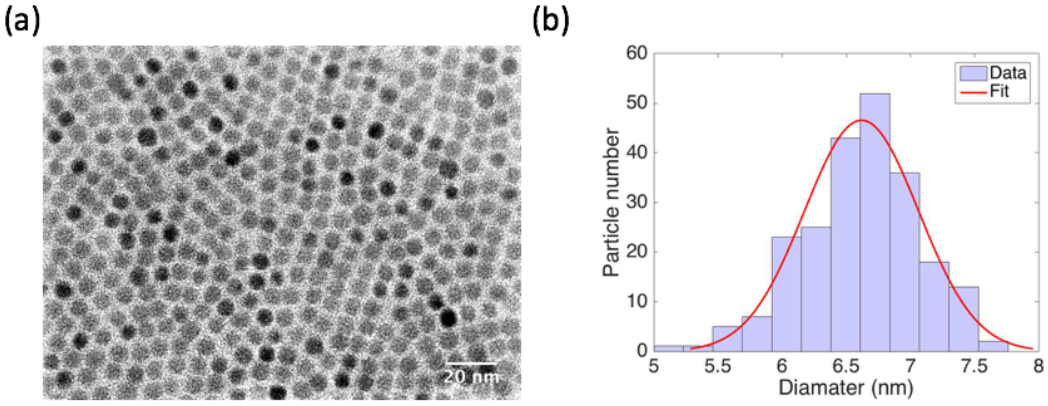

Figure 2.11 (a) TEM image of PbS NCs. (b) Size distribution of 220 NCs obtained from TEM analysis.

2.4.2 Substrate patterning

Substrates for inkjet printing were prepared using the method from Minemawari et al.[15] Briefly, a silicon substrate with a layer of oxide SiO_2 ~100 nm was coated with hexamethyldisilazane (HMDS) using a YES Vapor Prime Oven. A layer of 2 μm photoresist S1818 was spin coated at 4000 RPM for 1 min and baked at 115 °C for 1 min. It was then exposed to an ABM Contact Aligner (365-405 nm) for 5 s under a mask written with different shapes of 100-1000 μm size. After developing using a Hamatech machine with 726 Metal Ion Free for 1 min, the unmasked regions were plasma cleaned and deposited with monolayer of 3-mercaptopropyltrimethoxysilane (MPTMS), or 2-[methoxy(polyethylenoxy)propyl]trichlorosilane (PEG) of ~2 nm, using a molecular vapor deposition tool (MVD100).

2.4.3 Inkjet printing of PbS NCs

We use a Fujifilm Dimatix printer to print PbS NCs suspended in anhydrous 1,2-dichlorobenzene (DCB). The cartridge has 16 piezo-actuated nozzles – each can be adjusted individually. A voltage driven membrane behind the nozzle deforms to fill the chamber, dispenses the ink and recovers after jetting. The viscosity of DCB is 1.3 cP at room temperature. By adjusting the filling voltage and duration, stable jetting was realized with an error of droplet displacement of 20 μm from the printing height of 250 μm. The firing voltage was set at ~15 V and the typical jetting velocity was 1.5-3 m/s. Each droplet was 5-10 pL and the jetting frequency was 5 kHz.

3 Self-assembly of PbS NCs at fluid interface

3.1 Introduction

Self-assembly of NCs is driven by electrostatic, van der Waal and entropic forces.[35] As the NCs assembly ordering on a solid substrate is limited by the solvent evaporation, Dong et al.[19] reported the method of liquid-air interface assembly. The NCs precursor is placed on a subphase immiscible with the NC solvent. The liquid subphase provides a higher mobility for NCs to arrange during solvent evaporation, and superlattice grain size can approach micrometer.[19,20,31]

The assembly and attachment of PbSe NCs was demonstrated by Evers et al.[14] to form linear, square and hexagonal geometries. They showed that by adjusting the concentration of NCs in their suspension, the concentration of oleic acid ligands in the subphase, or by changing the reaction temperature, different geometries can be obtained. The NC facets that are bonded together in the superlattice was determined by the orientation of NCs at fluid interface.[14]

The liquid subphase also acts as a reservoir where chemicals can be delivered to adjust the reaction conditions. Whitham et al.[10] synthesized PbSe NC square superlattices by adding ethylenediamine (EDA) into ethylene glycol (EG) to strip ligands from (100) facets of the NCs and induce bonding connections. Similarly, Wu et al.[31] performed in situ ligand exchange by adding the 3-mercaptonpropionic acid (MPA) in the subphase and showed that the assembly ordering was preserved during ligand exchange on a liquid substrate.

The liquid-air interface assembly in the big Teflon trough allows thin film transfer onto flexible substrates.[19,20] However, it causes significant materials waste and the transfer process may induce extra damages to the thin films.

The problem may be overcome by inkjet printing that obtains precise registry of the nanostructured thin film on a small area. Similar to the idea of fluid interface assembly of NCs, Minemawari et al.[15] reported the fabrication of C_8-BTBT thin film using an anti-solvent coupled inkjet printer. The sequential printing of an anti-solvent and organic semiconductor formed single crystal thin film by controlling the crystallization before solvent evaporation. To form uniform thin film on the micropattern, complete wetting of solvent on the subphase needs to be realized. Noda et al.[36] used a high speed camera to capture the contact dynamics of two miscible solvents that was strongly influenced by the relative surface tension and jetting conditions.

In the following section we demonstrate the assembly of PbS NCs with two-phase printing - the printing of EG as a liquid subphase and NCs suspension on top. We designed the pattern to be of different shapes and confined the droplets in partial regions. A thin layer of NCs assembly was characterized by X-ray scattering but did not realize full coverage to the pattern. Crystallization into fcc structures occurred with more materials printed. However, the formation of a stable fluid interface is still of challenges due to the high speed of jetting in most inkjet printing techniques.

3.2 Results and Discussion

3.2.1 Inkjet printing of PbS NCs on a liquid subphase

We transferred the previous Teflon trough NC assembly[19] onto a Dimatix inkjet printer. To deposit the EG subphase on a flat substrate, the surface was patterned with hydrophilic group on confined areas. Following the substrate preparations described in chapter 2, the unmasked regions were treated with UV-Ozone for 20 min and small chains of Si-OH hydrophilic groups were grown on the pattern. The photoresist was then removed by washing with acetone, ethanol and deionized water for 1 min each.

EG is a liquid of viscosity of 16.9 cP at room temperature. The waveform was adjusted to dispense EG from a height of 400 μm above the substrate at the velocity of 6 m/s. The hydrophilic pattern on the SiO_2 substrate was aligned using a fiducial camera on the Dimatix printer and the platform temperature was set at 28 °C. Each drop of EG ink (~10 pL) had a diameter of 70 μm. The droplet spacing was set as 35 μm. The typical printing volume of EG was about 20-50 nL on most patterns. NCs ink was prepared by suspending PbS NCs in DCB at 20 mg/ml. The jetting speed of NCs solution was 1-2 m/s. Each droplet was ~5 pL at a spacing of 5 μm. Figure 3.1(a) shows the image captured immediately after 1 nL of NCs were printed on 23 nL of EG at the protuberant area (the blue cross). As more materials were printed (2.5 nL), we see from figure 3.1(b) some turbulent mixing.

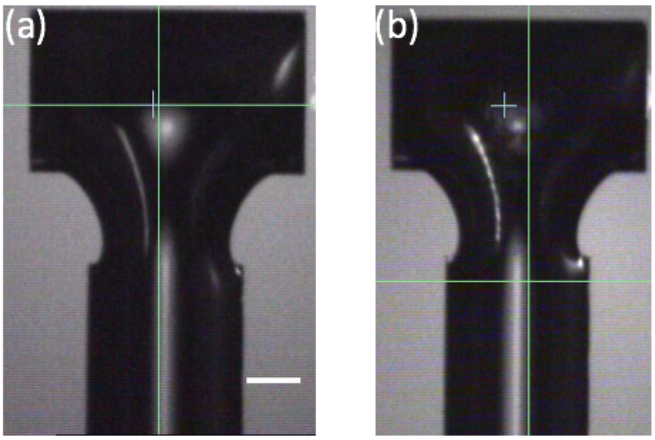

Figure 3.1 Optical images of the protuberant pattern covered with 23 nL of EG and overdeposited with (a) 1 nL and (b) 2.5 nL of PbS NCs solution. The scale bar is 100 μm.

Figure 3.2(a-b) show GISAXS data the deposit before and after drying of the subphase. The optical images of the samples are shown in the inset. The wet sample was measured within 30 min of printing. From the tilted rod and weak scattering patterns, we infer that some periodic arrangements were formed. The dried sample was measured 15 min afterwards showing better grain orientations with respect to the substrate. The average distance between neighboring NC surfaces was ~3.5 nm, indicating that ligands were maintained on NC surfaces.

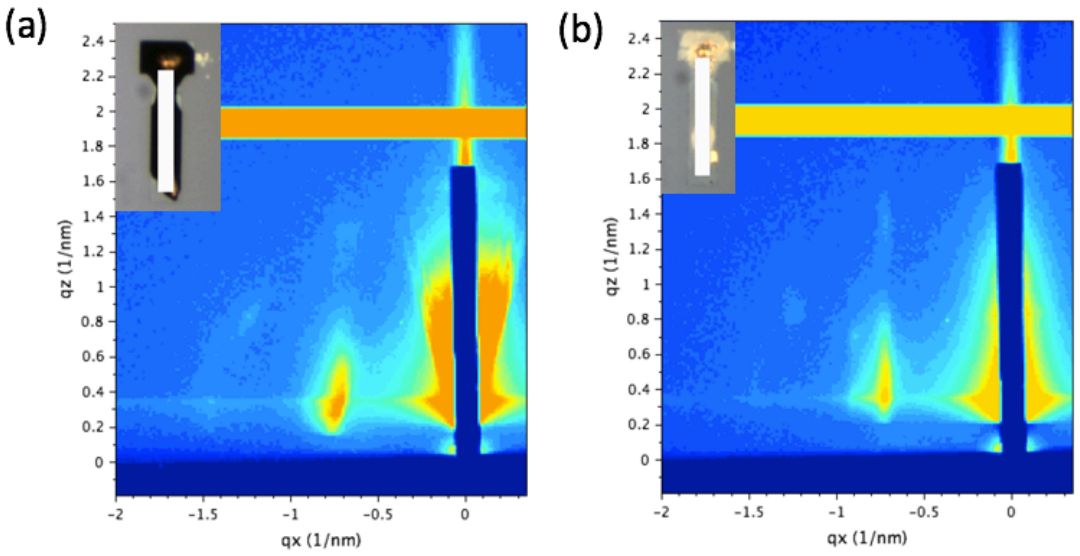

Figure 3.2 GISAXS pattern of the deposit formed with PbS NCs on EG subphase (a) before and (b) after the drying of EG. Inset is the optical image of the sample during measurements.

The EG subphase is relatively inert to the NCs and mainly provides a liquid support for NCs to arrange with a higher mobility during its solvent evaporation. Longer exposure of NCs to the subphase, however, may cause ligand stripping and destabilize the particles. In the conventional assembly experiments, the thin film is transferred to other substrates from the interface layer, and thus the assembly is mainly controlled simply by the solvent evaporation. In the inkjet printing, the subphase affects the NCs assembly to a larger extent due to the curvature of the droplet on a flat substrate, contact dynamics during printing, and the evaporation time before the thin film is attached to substrate.

The liquid contact of the microdroplet is affected by the surface tension and the volume of two phases.[36] In our experiment when EG volume was below a threshold (e.g., 20 nL on the area of 2 mm^2), the coverage of the pattern by subphase was perturbed during NCs jetting and the entire

deposit shrank into a circular shape as shown in figure 3.3(a). Increasing the volume of subphase (60 nL on the same pattern) preserved its coverage on substrate as shown in figure 3.3(b). Thus, the subphase deposition may not be optimized for crystal growth but for stabilizing the interface. Reducing the jetting velocity might alleviate the problem to some extent, but is limited by the hardware at current stages.

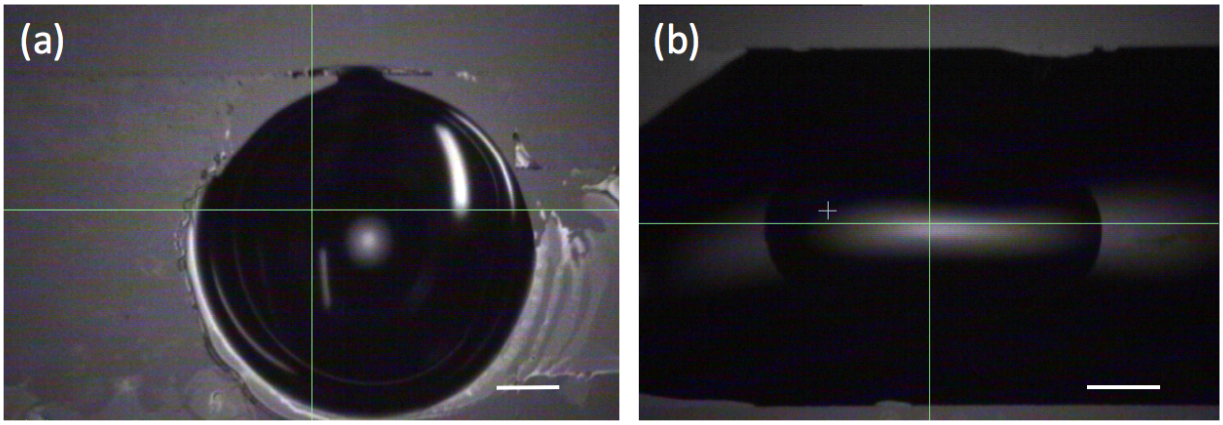

Figure 3.3 Optical images of the liquid contact after depositing 11 nL of NCs/DCB on (a) 20 nL and (b) 60 nL of EG on a pattern of area 2 mm^2. Scale bar is 200 μm.

3.2.2 Thin film formation at fluid interface

Figure 3.4 (a-c) show the GISAXS patterns of the thin films deposited with decreasing amount of NCs (2.5 nL, 2 nL and 1.5 nL) printed on the protuberant area of the pattern. Figure 3.4(d) illustrates the flow of NCs solution from the confined area to the longer regions. The scattering patterns in figure 3.4(a,b) were indexed to the fcc structure with a lattice constant of 13.5 nm and the (111) plane of the superlattice parallel to substrate. Figure 3.4(e) shows the integrated

intensities along q_x for different samples. The grain size in the in-plane direction was estimated to be ~85 nm. The distance between NCs surfaces decreased from 3 nm to 2.6 nm as the PbS NCs volume decreased from 2.5 nL to 1.5 nL.

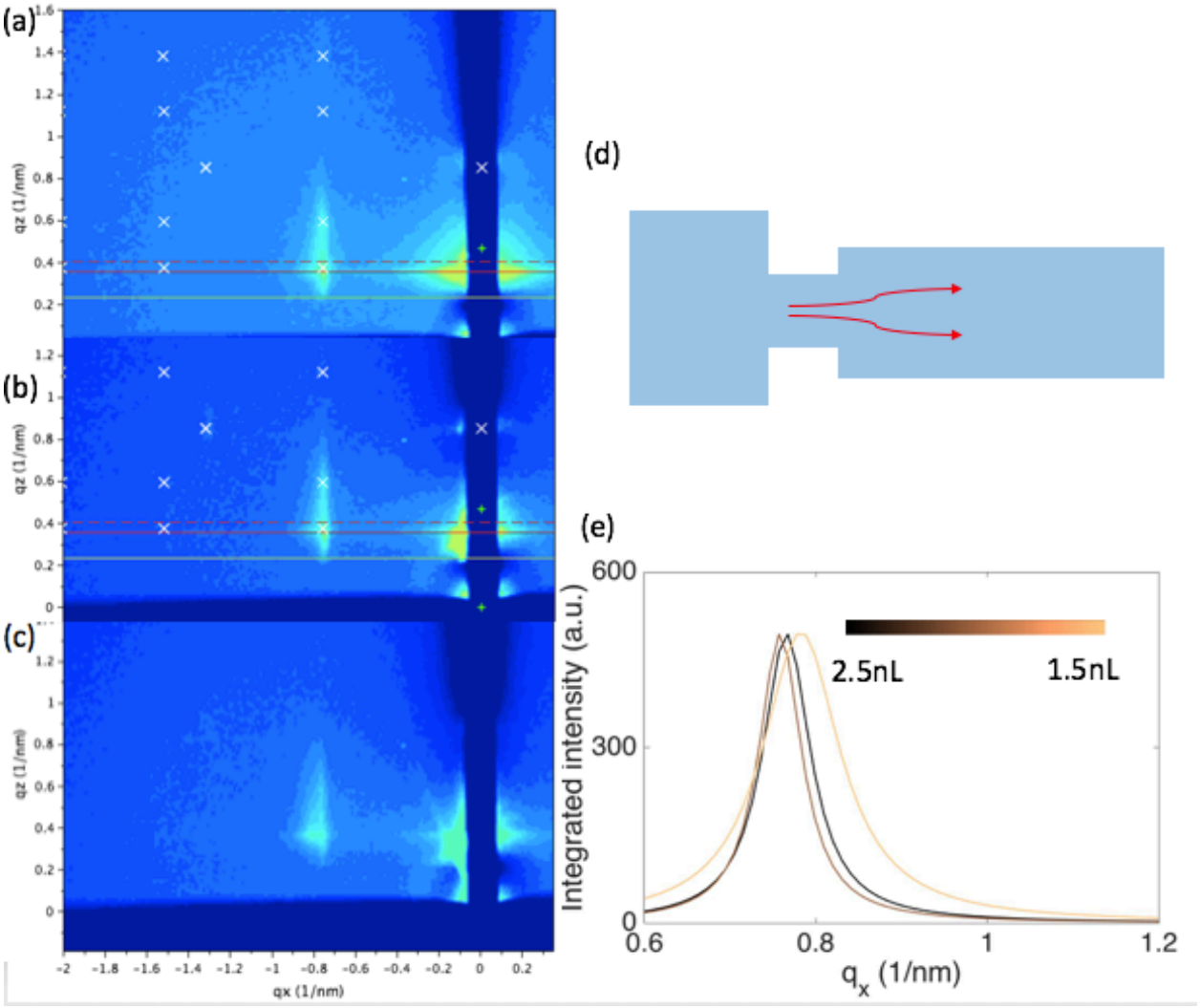

Figure 3.4 (a-c) GISAXS patterns of the deposit with decreasing NCs ink volume. (d) Illustration of the pattern shape and liquid flow. (e) Vertically integrated intensities of the scattering pattern in (a-c).

The trend of reduced particle spacing as NC volume decreased was also observed on a circular pattern. Figure 3.5(a-d) show the GISAXS data of thin films printed with NCs solution (3.5 nL to 2 nL at 20 mg/ml) on 20 nL of EG in a circular shaped hydrophilic pattern illustrated in figure 3.5(e). Figure 3.5(f) plots the the scattering intensities along q_x. The Lorentzian peak near 0.75nm^{-1} and 0.88nm^{-1} corresponded to the distance between NC surfaces, δ, of 3.1 nm and 1.6 nm. The grain size estimated from the main peak was ~100 nm for sample (a).

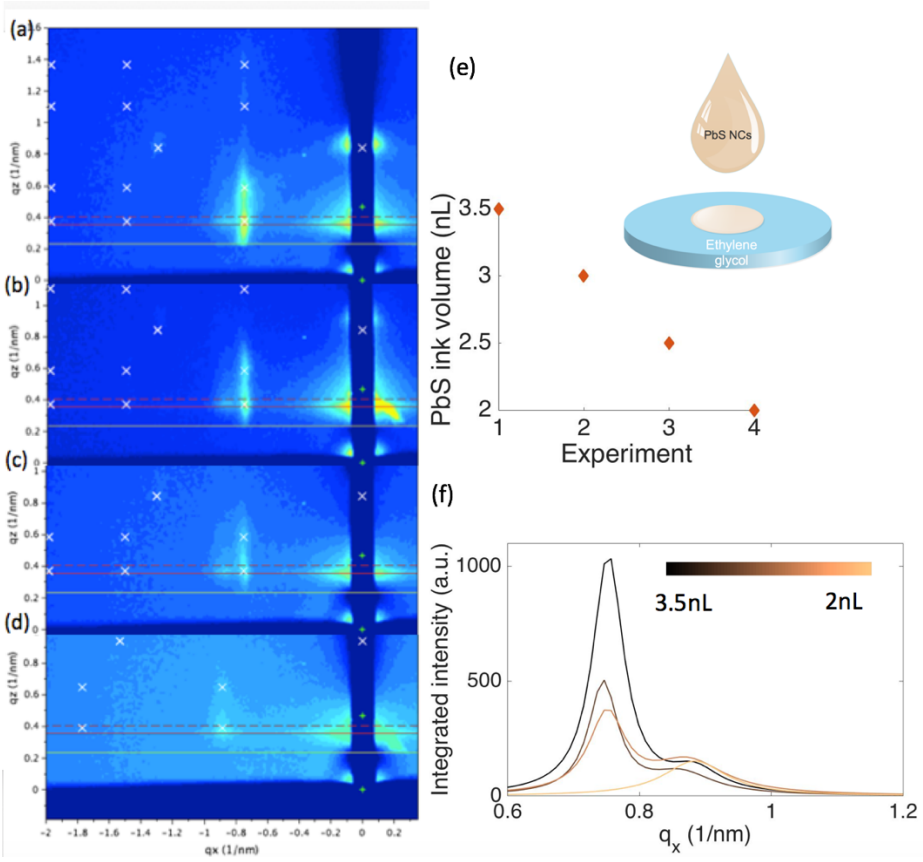

Figure 3.5 (a-d) GISAXS pattern of the thin film on a circular pattern formed with decreasing NCs ink volume. (e) Illustration of PbS NCs printing on EG. The NCs ink volume decreased from 3.5 nL to 2 nL on different samples. (f) Vertically integrated intensities of the pattern (a-d).

Figure 3.6(a-d) show SEM images of the deposit on the circular pattern. We found that the film morphologies varied significantly. Near the regions where NCs were printed, figure 3.6(b) shows that thin layers were formed. In figure 3.6(c), the darkest areas were the fusing of NCs, white dots were aggregation of ligands and the remaining areas were the bare substrate. The ligand aggregates in the intermediate regions shown in figure 3.6(c) indicates that as the NC ink spread outwards and became thinner on the subphase, the surfaces of NCs were heavily destabilized. The mesh structures in the outmost regions shown in figure 3.6(d) were due to sinking of the NCs suspension into subphase and its slow diffusion in EG. The NCs arrangement was not resolved in these SEM images possibly due to the surface destabilization caused by EG, or that the ordered structures were below the thin films seen on the top layer.

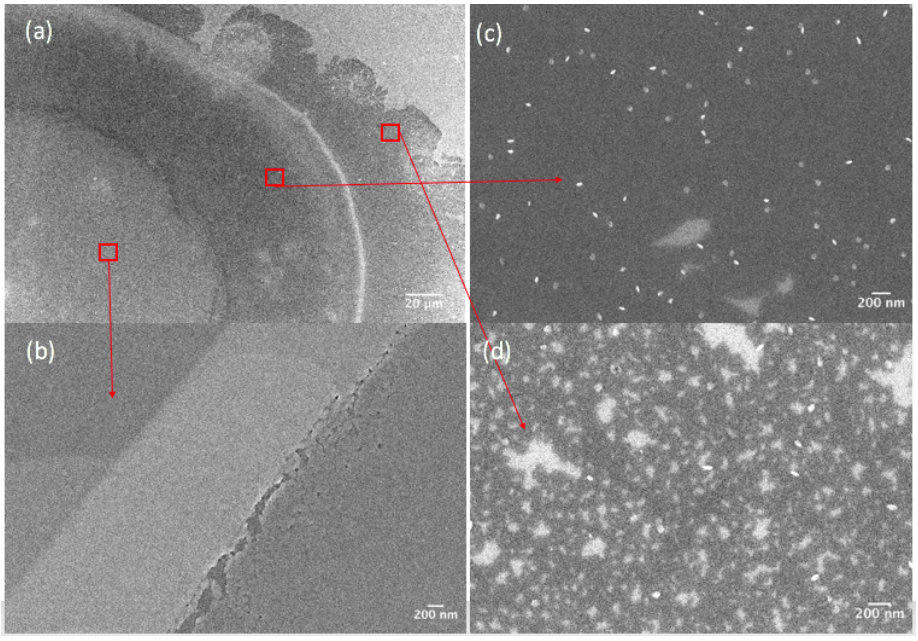

Figure 3.6 (a-d) SEM images of the PbS NCs assembly at fluid interface.

3.2.3 Formation of multi-layered superlattice

To investigate the crystalline structures formed in the experiments above, we scaled up the printing volume by an order of magnitude. Specifically, 60 nL of PbS NCs solution (15 mg/ml, core size of 4.8 nm) was printed on 160 nL of EG using a large pattern of dimension 1 mm × 2 mm. The deposit was dry in 2 hours. A control experiment was done without the subphase, and the solvent was dried within 1 min. Figure 3.7 (a-b) illustrate the assembly environment.

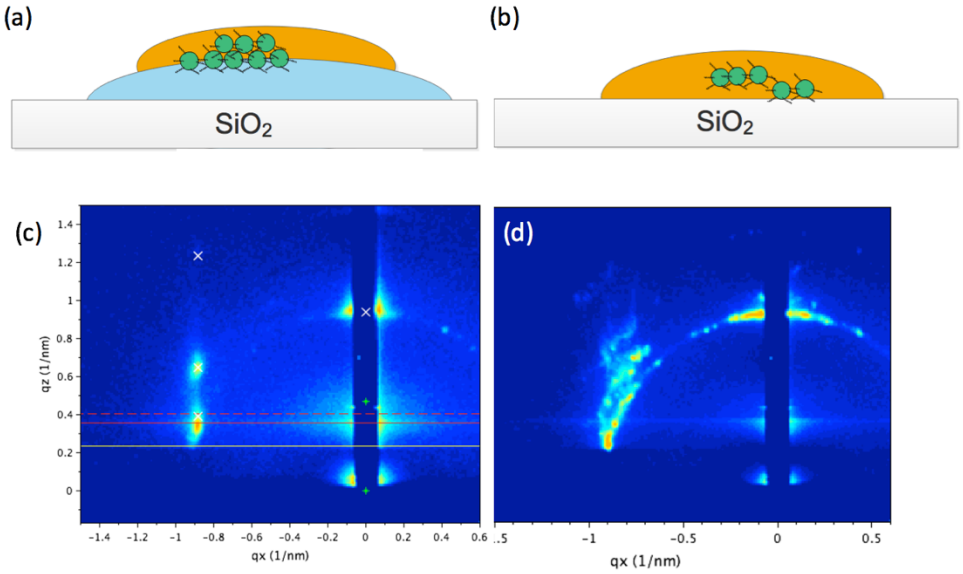

Figure 3.7 Schematic of NCs assembly on (a) liquid and (b) solid surface. (c-d) GISAXS pattern of the NCs superlattice formed according to (a-b).

Figure 3.7(c) is the GISAXS data of the NCs assembly formed at fluid interface averaged over 500 μm in width. It was indexed to a fcc structure with a lattice constant of 11.6 nm. The (111) plane of the superlattice was parallel to the substrate. Neighboring NC surfaces were separated by 3.4 nm. Figure 3.7(d) is the GISAXS data of the deposit directly printed on the Si/SiO_2

substrate. The ringlike patterns indicate that the grains were oriented randomly. This may be caused by homogeneous nucleation that occurred in the bulk liquid phase.

For the GISAXS data in 3.7(c), the scattering intensities along q_x and q_z were plotted in figure 3.8 (a-b). The first peak along q_x was fitted into a Lorentzian model near q_x= 0.9 nm^{-1} and the grain size was calculated to to be ~170 nm. This is much larger than the grain size of the thin film printed directly on a solid substrate.

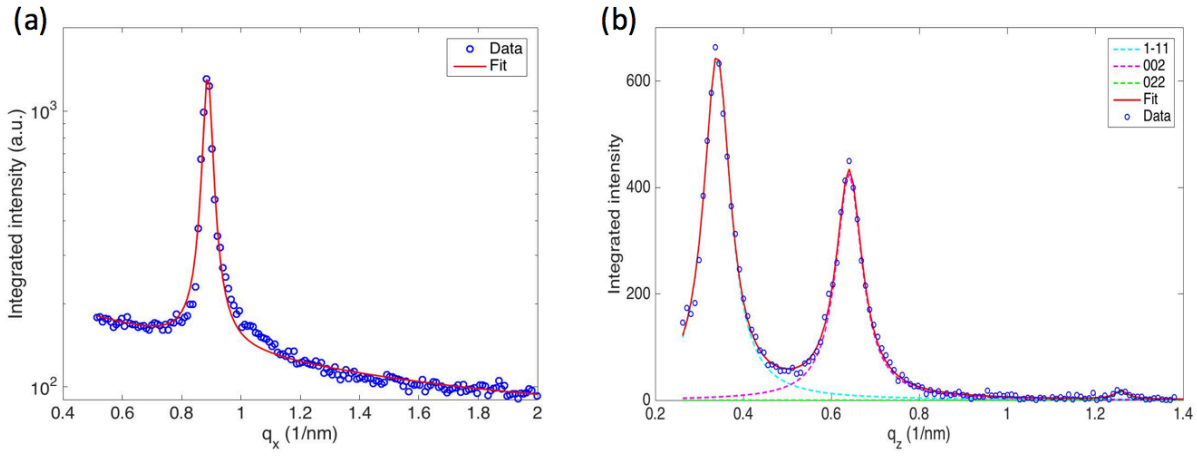

Figure 3.8 Integrated intensities along (a) in-plane and (b) out-of-plane directions of the pattern shown in figure 3.7(c).

In the q_z direction, we fitted the scattering intensity to three Lorentzian peaks, the first two gave an estimate of the domain size of 77 nm. The multi-layer growth was guided by the interface layer and grain orientations were preserved during the drying of the subphase. As the spreading of the NC suspension was non-uniform, the thickest deposited formed near the center. However, by performing the X-ray scattering measurements in multiple locations on the pattern, we found that the fcc superlattice was not limited to the big aggregates near the center. Instead, the

interface mediated assembly of NCs into a fcc superlattice was formed in wide areas of the pattern.

3.3 Conclusions

Incorporating the idea of using a fluid substrate to enhance NC mobility, and the inkjet printing technique with precise spatial and dispensed volume control, we demonstrated the liquid interface assembly of PbS NCs on the hydrophilic pattern of size ~1-2 mm^2. The formation of the contact layer between solvent and nonsolvent was adjusted by the surface tensions, the volume ratio, and the jetting speed.

Although the fluid interface was not fully stabilized, the superlattice grown from the interface layers was characterized to have grain size ~170 nm. This is much larger than what we achieved by direct printing on a solid substrate with optimal drop settings (discussed in chapter 2). The assembled layer at fluid interface assisted with the growth of multi-layered structures into 3d fcc packing.

While the assembly ordering has been improved significantly on fluid interface (in both Teflon trough and inkjet printing experiments shown here), the nucleation and growth mechanisms of the NCs superlattice are not well understood. Conducting fluid interfacial assembly on the micropattern with directed fluid flow may enable a higher level of control of the kinetic factors during the self-assembly. Further investigation in the superlattice growth guided by fluid diffusion may give insights into single crystal growth and advance QDS fabrication.

4 Chemical treatments of NCs thin films

4.1 Introduction

As-synthesized semiconductor NCs are capped by long chain of ligands. While ligand interaction plays an important role in the design of functional materials, the separation between NCs limits the carrier mobility. Replacement of the long chain molecules into shorter ligands, or to inorganic ligands, enhances the interdot coupling.[31,37]

The epitaxial connection between neighboring facets creates connected-but-confined structure of quantum dots solids (QDS).[25] Lead chalcogenide assembly can be transformed from hexagonal structures to square lattice upon partial ligand removal.[10,25] The facet selectivity in ligand stripping is due to the binding energy differences of oleic acid and lead on (111) and (100) planes of the NCs.[35] Interestingly Evers et al.[14] reported the phase transformation of PbSe NCs into other linear, square and hexagonal symmetries, and the distinct phases appeared with precise control of the reaction temperature, ligand densities and NCs concentrations.

Walravens et al.[38] observed that the epitaxial bonding was favored under stoichiometric conditions of the neighboring facets that could be realized by introducing chalcogenide or amine additives. The replacement of oleic acids by chalcogenide salts was also reported by Oh et al.[39] where they demonstrated that the post-deposition growth of chalcogen-rich and lead-rich layers on NCs induced atomic fusion between (100) plane.

Variations in the bonding width between NCs limit the charge delocalization in the QDS thin film.[10] Current approaches of triggering oriented attachment at fluid interface by injecting amine additives to the subphase cannot avoid the problem of mechanical perturbation and uncontrolled liquid diffusion.

Phase transformation on a micropattern has the potential of minimizing uncertainties in liquid diffusion. To investigate the feasibility of inducing bonding connections in the assembled structures fabricated using inkjet printing, we first characterize the surface stabilities of these NCs. We used the Fourier transform infrared (FTIR) spectroscopy and SEM to characterize the ligand coverage and structural changes after antioslvent treatment of the NCs thin film, and found that although the inkjet printing preserved ligand densities on NCs, the surface bound ligands became destabilized and were more vulnerable to ligand stripping agents.

4.2 Results and Discussion

4.2.1 NCs surface ligands characterization

We measured FTIR spectra of PbS NCs thin films as-deposited and after 2 min of ethanol wash. Ethanol is an antisolvent that slowly strips off the ligands from PbS NCs. It is used for washing particles after synthesis to remove excessive oleic acids.

About 10 μl of the PbS NCs suspension in DCB (~5 mg/ml) was drop casted onto a glass slide. Another set of films were prepared by inkjet printing using the same batch of materials. All samples were dried in air at room temperature. FTIR spectra were measured using a Bruker Hyperion spectrometer in the transmission mode. A blank glass slide was used as background.

Figure 4.1 shows the absorption peak of C-H vibrations near 2850-2950 cm^{-1} and the exciton peak of PbS NCs near 6000 cm^{-1}. All spectra were normalized at the exciton peak. The intensity of C-H vibrational signal in printed film was higher than the drop casted one. After the ethanol wash however, the integrated intensity of the C-H peak showed a 27% and 42% decrease for the drop casted sample and printed sample respectively. Also, we observed from the data without normalizing that the reduction in the absorption intensity of PbS NCs on printed films was twice than the drop casted deposit after ethanol wash, indicating weaker attachment of NCs to the substrate.

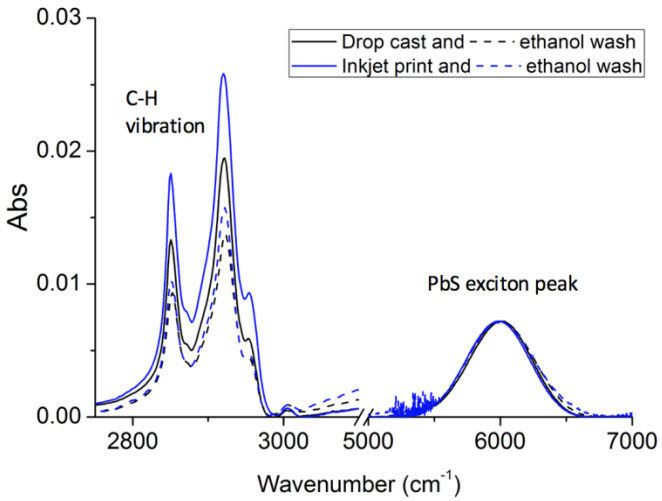

Figure 4.1 FTIR spectra of the PbS NCs thin film on a glass slide prepared by drop casting (black lines) and inkjet printing (blue lines), followed by ethanol treatment.

The higher C-H intensity from the printed film might be caused by other organic residues in the cartridge. While this introduced some error to the comparison between two deposition methods, the ligand detachment by ethanol was shown to be more effective in the printed samples.

4.2.2 Amine treatment of PbS NCs thin film

The thin films of PbS NCs prepared by drop casting and inkjet printing were dipped into ethylenediamine (EDA) solution at various concentration for 1 min. The precursor was formed by dissolving 25 μl of EDA into 1.5 ml of ethanol, and further diluted by a factor of 2 and 10.

Figure 4.2(a-d) are SEMs images the PbS NCs assembly prepared by the drop casting followed by EDA treatment at EDA/ethanol volume fraction of 0.17%, 0.8% and 1.7%. The void fraction increased due to ligand loss, but assembly ordering was preserved for EDA concentration below 0.8% in figure 4.2(b,c).

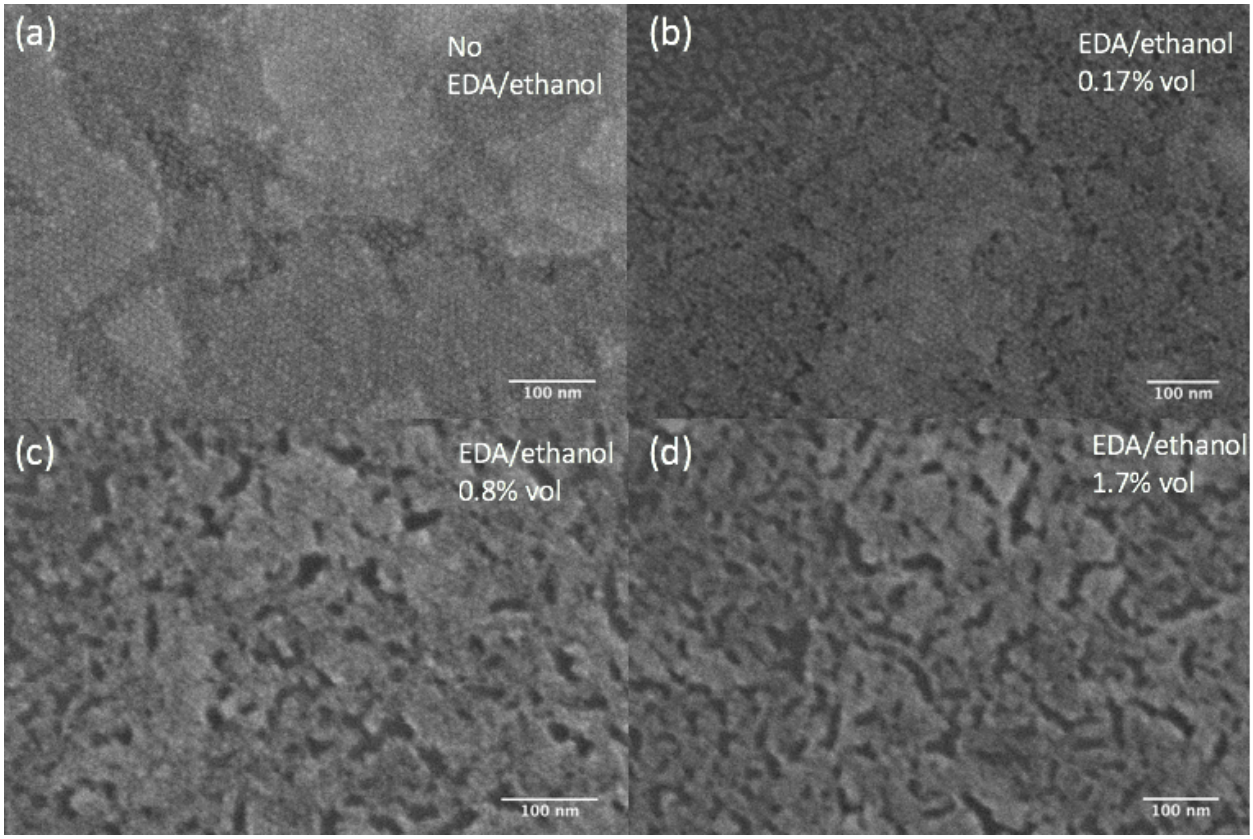

Figure 4.2 (a-d) SEM images of the NCs thin film prepared by drop casting and EDA/ethanol treatment at different concentrations.

The SEM images before and after EDA treatment of the printed films are shown in figure 4.3(a-b). The black regions in figure 4.3(b) are substrate, and the grey regions are PbS NCs residues after amine treatment. We see that a large fraction of the deposit was washed away. The

assembly ordering was lost entirely, left with scattered aggregates. This is consistent with FTIR results. The NCs in the printed samples were more easily detached from the substrate.

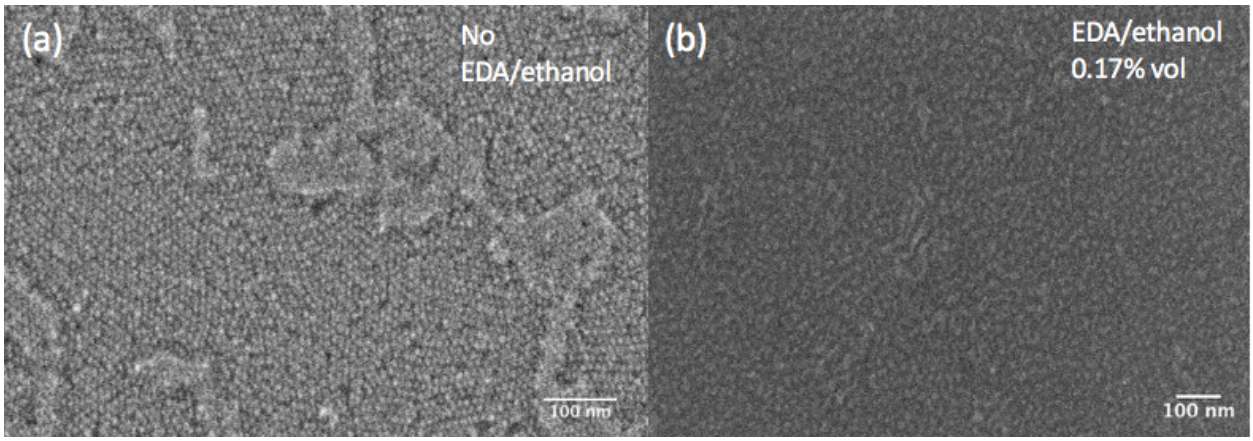

Figure 4.3 SEM images of NCs thin film on a silicon substrate (a) as-printed and (b) after EDA/ethanol treatment.

The surface bound ligands on NCs are in equilibrium with the free ligands. Moreels et al.[40] reported the typical exchange rate over 200/s for PbS NC capped by oleylamine. In chapter 2-3, we showed that in the printed thin films, NCs were almost separated by two ligand shells. Also the multi-layered structures were consistently indexed to fcc structures, which would occur for NCs with well-preserved ligands.[35] Thus it is likely that the jetting process did not filter the ligands but the destabilization came from the shearing force at the nozzle or the oxidation of NCs.

4.3 Conclusions

In this chapter, we characterized the surface stability of NCs during the thin film processing. We found that although the ligands were preserved during the self-assembly after inkjet printing, a larger fraction of them was reduced by ethanol treatment as compared to the thin films prepared in the conventional drop casting method. The situation might be more severe in amine treatment as the assembly ordering was entirely lost in the printed thin film.

Careful study of the ligand chemistry is needed in the design of NCs inks that ensures their stability and printability. On the other hand, thin film processing needs to take into consideration the surface sensitivity of nanomaterials. Input from both aspects is critical for the integration of colloidal materials into solid state devices.

5 Summary and outlook

The work presented here is the first trial using inkjet printing to fabricate NCs thin films with periodic arrangement of the NC building blocks. The PbS NCs capped by oleic acids were printed on liquid-solid and liquid-liquid interface using a Dimatix Materials Printer.

Uniform thin films with monolayer to bilayer coverages were obtained over the area of ~0.5 mm^2 by direct printing on a silicon substrate. The range of order was limited to ~50 nm. Depositing a liquid subphase yielded a better control of the NCs diffusion. The superlattice of NCs that formed on the fluid interface was characterized by GISAXS to be fcc structures, with in-plane grain size ~170 nm. The deposit obtained on the substrate after the drying of the subphase showed significant thickness variations across the pattern caused by the incomplete wetting of the NCs suspension on subphase. The situation could be improved with a more stable jetting system enabling wider solvent selections.

Cao et al.[41] demonstrated the fabrication of carbon nanotube thin film transistor with all layers printed by an aerosol jet printer. The printed gate dielectric was shown to have negligible hysteresis and low threshold voltage.[41] While the printing technique has advanced towards higher resolution and faster speed, from a chemical perspective however, QDS formation is not a simple deposition but requires chemical perturbations at different stages. The design of the printing system incorporating this concept would have impact to the fabrication of complex functional materials.

To impose a higher degree of control on nanomaterials integration, directing the assembly of NCs using an external field is another subject under research. Ryan et al.[42] observed the alignment of CdS nanorods with electric field during the evaporation driven assembly. Singh et al.[43] demonstrated the formation helical superstructures composed of magnetite NCs as building blocks. The assembly was conducted at liquid-air interface with an external magnetic field that enabled the alignment of magnetic dipoles of NCs.[43] Recently Yu et al.[44] used electric field to drive the assembly of silver nanoparticles without solvent evaporation. The interaction between external fields and the NCs as a perturbation to the intrinsic driving forces in self-assembly would offer extra tools for structural control and increase fabrication efficiency.

The printing technique provides systematic control of the assembly environment that makes it an idea tool to unravel the assembly kinetics. We envision its potential to improve the performance of NCs based devices by constructing high quality superlattices on the micropattern. Directing the self-assembly of NCs using external fields would allow a higher level of control of the complex structures formation.

6 References

(1) Brus, L. E. *J. Chem. Phys.* **1984**, *80*.
(2) Wise, F. W. *Acc. Chem. Res.* **2000**, *33* (11), 773–780.
(3) Yang, Z.; Voznyy, O.; Liu, M.; Yuan, M.; Ip, A. H.; Ahmed, O. S.; Levina, L.; Kinge, S.; Hoogland, S.; Sargent, E. H. *ACS Nano* **2015**, *9* (12), 12327–12333.
(4) Sun, L.; Choi, J. J.; Stachnik, D.; Bartnik, A. C.; Hyun, B.; Malliaras, G. G.; Hanrath, T.; Wise, F. W. **2012**, *7* (May), 369–373.
(5) Iacovo, A. De; Venettacci, C.; Colace, L.; Scopa, L.; Foglia, S. *Sci. Rep.* **2016**, *6*.
(6) Zhao, T.; Goodwin, E. D.; Guo, J.; Wang, H.; Diroll, B. T.; Murray, C. B.; Kagan, C. R. *ACS Nano* **2016**, *10*, 9267–9273.
(7) Hines, M. A.; Scholes, G. D. *Adv. Mater.* **2003**, *15* (21), 1844–1849.
(8) Bian, K.; Richards, B. T.; Yang, H.; Bassett, W.; Wise, F. W.; Wang, Z.; Hanrath, T. *Phys. Chem. Chem. Phys.* **2014**, *16*, 8515–8520.
(9) Weidman, M. C.; Smilgies, D.-M.; Tisdale, W. A. *Nat. Mater.* **2016**, *15* (March), 1–8.
(10) Whitham, K.; Yang, J.; Savitzky, B. H.; Kourkoutis, L. F.; Wise, F.; Hanrath, T. *Nat. Mater.* **2016**, *15* (February), 1–8.
(11) Reich, K. V.; Shklovskii, B. I. *ACS Nano* **2016**, *10*, 10267–10274.
(12) Kalesaki, E.; Delerue, C.; Smith, C. M.; Beugeling, W.; Allan, G.; Vanmaekelbergh, D. *arXiv* **2015**.
(13) Kalesaki, E.; Evers, W. H.; Allan, G.; Vanmaekelbergh, D.; Delerue, C. *Phys. Rev. B - Condens. Matter Mater. Phys.* **2013**, *88* (11), 1–9.
(14) Evers, W. H.; Goris, B.; Bals, S.; Casavola, M.; De Graaf, J.; Roij, R. Van; Dijkstra, M.; Vanmaekelbergh, D.; Porcel, S.; López-carrillo, V.; García-yebra, C.; Antonio, M. *Nano Lett.* **2013**, *13* (6), 2317–2323.
(15) Minemawari, H.; Yamada, T.; Matsui, H.; Tsutsumi, J.; Haas, S.; Chiba, R.; Kumai, R.; Hasegawa, T.; Sun, M.; Paciga, J. E.; Feldman, R. I.; Yuan, Z. Q.; Coppola, D.; You Yong Lu; Shelley, S. A.; Nicosia, S. V.; Cheng, J. Q. *Nature* **2011**, *475* (7356), 364–367.
(16) Diao, Y.; Tee, B. C.-K.; Giri, G.; Xu, J.; Kim, D. H.; Becerril, H. a; Stoltenberg, R. M.; Lee, T. H.; Xue, G.; Mannsfeld, S. C. B.; Bao, Z. *Nat. Mater.* **2013**, *12* (7), 665–671.
(17) Park, S.; Giri, G.; Shaw, L.; Pitner, G.; Ha, J.; Hoon, J.; Gu, X.; Park, J. *PNAS* **2015**, *112* (18), 5561–5566.
(18) Diao, Y.; Shaw, L.; Bao, Z.; Mannsfeld, S. C. B. *Energy Environ. Sci.* **2014**, *7* (7), 2145–2159.
(19) Dong, A.; Chen, J.; Vora, P. M.; Kikkawa, J. M.; Murray, C. B. *Nature* **2010**, *466* (7305), 474–477.
(20) Paik, T.;Yun, H.; Fleury, B.; Hong, S.-H.; Jo, P. J.; Wu, Y.; Oh, S. J.; Cargnello, M.; Yang, H.; Murray, C. B.; Kagan, C. R.; Paik, T.; Yun, H.; Fleury, B.; Hong, S.-H.; Jo, P. S.; Wu, Y.; Oh, S.-J.; Cargnello, M.; Yang, H.; Murray, C. B.; Kagan, C. R. *Nano Lett.* **2017**, *17* (3), 1387–1394.
(21) Wu, M.; Bodnarchuk, M. I.; Kovalenko, M. V; Pichler, Ḱ. S.; Fritz-popovski, G. *ACS Nano* **2010**, *4* (1), 423–431.
(22) Heitsch, A. T.; Patel, R. N.; Goodfellow, B. W.; Smilgies, D. M.; Korgel, B. A. *J. Phys. Chem. C* **2010**, *114* (34), 14427–14432.

(23) Jung, B.; Lim, A.; Lee, W. H.; Lee, H. S.; Lee, J. H.; Park, Y. D.; Cho, K. *Adv. Funct. Mater.* **2008**, *18*, 229–234.
(24) Li, H.; Cha, J. J.; Cui, Y.; Chung, J. W.; Lee, S. Y.; Bao, Z. *JACS* **2012**, *134*, 2760–2765.
(25) Baumgardner, W. J.; Whitham, K.; Hanrath, T. *Nano Lett.* **2013**, *13* (7), 3225–3231.
(26) Choi, J.-H.; Wang, H.; Oh, S. J.; Paik, T.; Sung, P.; Sung, J.; Ye, X.; Zhao, T.; Diroll, B. T.; Murray, C. B.; Kagan, C. R. *Science (80-.).* **2016**, *352* (6282), 205–208.
(27) Smilgies, D. M.; Blasini, D. R. *J. Appl. Crystallogr.* **2007**, *40* (4), 716–718.
(28) Smilgies, D. M. *J. Appl. Crystallogr.* **2009**, 1030–1034.
(29) Li, R.; Cornaby, S.; Kamperman, M. *J. Syncrhotron Radiat.* **2011**, *18*, 697–701.
(30) Choi, J.; Fafarman, A. T.; Oh, S. J.; Ko, D.; Kim, D. K.; Diroll, B. T.; Muramoto, S.; Gillen, J. G.; Murray, C. B.; Kagan, C. R. *Nano Lett.* **2012**, *12*, 2631–2638.
(31) Wu, Y.; Li, S.; Gogotsi, N.; Zhao, T.; Fleury, B.; Kagan, C. R.; Murray, C. B.; Baxter, J. B. *J. Phys. Chem. C* **2017**, *121*, 4146–4157.
(32) Sigman, M. B.; Saunders, A. E.; Korgel, B. A. *Langmuir* **2004**, *20* (3), 978–983.
(33) Hanrath, T.; Choi, J. J.; Smilgies, D.-M. *ACS Nano* **2009**, *3* (10), 2975–2988.
(34) Moreels, I.; Lambert, K.; Muynck, D. De; Vanhaecke, F.; Poelman, D.; Martins, J. C.; Allan, G.; Hens, Z. *ACS Nano* **2009**, *3* (10), 3023–3030.
(35) Choi, J. J.; Bealing, C. R.; Bian, K.; Hughes, K. J.; Zhang, W.; Smilgies, D.-M.; Hennig, R. G.; Engstrom, J. R.; Hanrath, T. *J. Am. Chem. Soc.* **2011**, *133* (9), 3131–3138.
(36) Noda, Y.; Minemawari, H.; Matsui, H.; Yamada, T.; Arai, S. *Adv. Funct. Mater.* **2015**, *25*, 4022–4031.
(37) Nag, A.; Kovalenko, M. V; Lee, J.; Liu, W.; Spokoyny, B.; Talapin, D. V. *J. Am. Chem. Soc.* **2011**, 10612–10620.
(38) Walravens, W.; De Roo, J.; Drijvers, E.; Ten Brinck, S.; Solano, E.; Dendooven, J.; Detavernier, C.; Infante, I.; Hens, Z. *ACS Nano* **2016**, *10* (7), 6861–6870.
(39) Oh, S. J.; Berry, N. E.; Choi, J.; Gaulding, E. A.; Lin, H.; Paik, T.; Diroll, B. T.; Muramoto, S.; Murray, C. B.; Kagan, C. R. *Nano Lett.* **2014**, *14*, 1559–1566.
(40) Moreels, I.; Justo, Y.; Geyter, B. De; Haustraete, K.; Martins, J. C.; Hens, Z. *ACS Nano* **2012**, No. 3, 2004–2012.
(41) Cao, C.; Andrews, J. B.; Franklin, A. D. *Adv. Electron. Mater.* **2017**, *1700057*, 1–10.
(42) Ryan, K. M.; Mastroianni, A.; Stancil, K. A.; Liu, H.; Alivisatos, A. P. *Nano Lett.* **2006**.
(43) Zubkov, M. A.; Kogan, S. M.; Levitov, L. S.; Spivak, B. Z.; Dzero, M.; Axt, V. M.; Kuhn, T.; Eckstein, M.; Werner, P.; Varma, C. M.; Klein, M. V; Varma, C. M.; Hoffmann, M. C.; Bartal, B.; Nelson, K. A.; Kampfrath, T.; Tanaka, K.; Nelson, K. A.; Shimano, R.; Watanabe, S.; Matsunaga, R.; Terai, H.; Takeda, M.; Uzawa, Y.; Wang, Z.; Aoki, H.; Uzawa, Y.; Wang, Z.; Goldman, A. M. *Science (80-.).* **2014**, *345* (6201), 380–382.
(44) Yu, Y.; Yu, D.; Orme, C. A. *Nano Lett.* **2017**, *17*, 3862–3869.